Infrared imaging diagnostics for intense pulsed electron beam

Cite as: Rev. Sci. Instrum. **86**, 083305 (2015); https://doi.org/10.1063/1.4928069
Submitted: 08 April 2015 . Accepted: 24 July 2015 . Published Online: 06 August 2015

Xiao Yu, Jie Shen, Miao Qu, Wenbin Liu, Haowen Zhong, Jie Zhang, Sha Yan, Gaolong Zhang, and Xiaoyun Le

Infrared imaging diagnostics for intense pulsed electron beam

Xiao Yu,[1,2] Jie Shen,[1,2] Miao Qu,[3] Wenbin Liu,[1,2] Haowen Zhong,[1,2] Jie Zhang,[1,2] Sha Yan,[3] Gaolong Zhang,[1,2] and Xiaoyun Le[1,2,a)]

[1]*School of Physics and Nuclear Energy Engineering, Beihang University, Beijing 100191, People's Republic of China*

[2]*International Research Center for Nuclei and Particles in the Cosmos, Beihang University, Beijing 100191, People's Republic of China*

[3]*Institute of Heavy Ion Physics, Peking University, Beijing 100871, People's Republic of China*

(Received 8 April 2015; accepted 24 July 2015; published online 6 August 2015)

Infrared imaging diagnostic method for two-dimensional calorimetric diagnostics has been developed for intense pulsed electron beam (IPEB). By using a 100-μm-thick tungsten film as the infrared heat sink for IPEB, the emitting uniformity of the electron source can be analyzed to evaluate the efficiency and stability of the diode system. Two-dimensional axisymmetric finite element method heat transfer simulation, combined with Monte Carlo calculation, was performed for error estimation and optimization of the method. The test of the method was finished with IPEB generated by explosive emission electron diode with pulse duration (FWHM) of 80 ns, electron energy up to 450 keV, and a total beam current of over 1 kA. The results showed that it is possible to measure the cross-sectional energy density distribution of IPEB with energy sensitivity of 0.1 J/cm^2 and spatial resolution of 1 mm. The technical details, such as irradiation protection of bremsstrahlung γ photons and the functional extensibility of the method were discussed in this work. [http://dx.doi.org/10.1063/1.4928069]

I. INTRODUCTION

Intense pulsed electron beams (IPEBs) have been developed for numerous applications such as surface modification of metals and alloys,[1,2] waste water treatment,[3] and nanopowder synthesis.[4] Many of these applications require large beam cross section (over 10 cm^2) with, simultaneously, high uniformity. And thus, it is necessary to measure the cross-sectional energy density distribution. Considering the characteristics of IPEB, different types of diagnostic techniques can be utilized. By using luminescence material and thermal films, it is easy to obtain brief description and distribution images, but it is difficult to get quantified data. Dosimetric films could provide high resolution images; however, their efficiency is largely confined by the high costs and the several hours of time spending on the image fixing. Unlike intense pulsed ion beam (IPIB) which requires charge neutralization for stable transportation, IPEB is composed mainly of electrons and it is not necessary for the heterogeneous charge stripping in detector design. As a result, the size of charge collector of Faraday cup used for IPEB detection is more flexible than the one used for IPIB. For electron stripping purpose, the Faraday cup used for IPIB detection requires magnetic field in the aperture, with the diameter of typically within 2 mm considering the Debye radius. Thus, the Faraday cup array for cross-sectional distribution diagnostics of IPEB is more convenient in comparison with that of IPIB. However, actually it is still quite challenging for satisfactory spatial resolution, and a total number of up to hundreds of detectors will be required. Moreover, it is also a complex problem to find a proper function that converts the beam current density into energy density satisfactorily. Calorimeter array method,[5] as a direct energy detecting method, has the similar troubles in spatial resolution and system complexity.

As a kind of direct energy density diagnostic method, thermal imaging method for the diagnostics of IPIB was first proposed in 1997[6] and developed afterwards.[7] Thermal imaging method using thin graphite plate as thermal sink for IPEB was also suggested.[8] It has been theoretically analyzed that the energy deposition depth of IPEB for surface treatment purpose, with typical electron energy of several tens of keV, is quite similar to one of the IPIBs with ion energy of several hundreds of keV.[9] As a result, the method is also applicable for IPEB.

However, for IPEB with electron energy of several hundred keV, since the range of electrons in metal becomes much greater, thicker target, which corresponds to lower cross-sectional energy resolution, is needed to stop electrons completely. Several efforts have been made with foamed polystyrene with low density and low thermal conductivity.[10] This method is quite creative, but it is still necessary to be improved when considering the accuracy which can be estimated theoretically. For example, when the target is heated in 5 s, only the heat radiation from the surface will lead to an error of over 2%.[9] When taking air convection cooling into account, the error will be greater. This method requires offline observing and measuring, making at least few seconds time delay inevitable.

This work begins with a brief description of infrared imaging diagnostics for IPEB. The IPEB-target interaction is simulated with Monte Carlo (MC) particle transportation code in order to evaluate the electron energy deposition. A two-dimensional axisymmetric heat transfer calculation is carried

a)Electronic mail: xyle@buaa.edu.cn

out for validation and error estimation of the method. Then, the results of infrared imaging diagnostics and some relevant technical details are discussed.

II. THEORETICAL AND MODELING

Similar to infrared imaging method for IPIB, the basic idea of the technique for IPEB is to use a thin metal target as the heat sink and suppose the energy distribution to be the function of temperature difference between cool and heated targets. To obtain a simple but satisfactory result in accordance with energy distribution, the following conditions should be met.

(1) The target film should be thick enough to get complete stopping of the electrons in the target.
(2) Thermal equilibrium should be established between front and rear surfaces.
(3) Lateral thermal conduction should be weak enough comparing with that in depth direction.
(4) No obvious target vaporization and ablation occur.

For the same particle energy, the range of electrons is much (almost two orders) greater than that of protons, so the complete stopping of electrons requires thicker targets. For the infrared imaging diagnostics, the thin metal target can serve as a matrix of tiny calorimeters, so the cross-sectional energy density distribution $U(x, y)$ of IPEB can be calculated with the following formula:

$$U(x, y) = C_V \cdot d \cdot \rho \cdot \Delta T(x, y), \tag{1}$$

where C_V is the specific heat of the target material, d is the thickness of the target, ρ is the density of the target, and $\Delta T(x, y)$ is the temperature change after IPEB irradiation. From Eq. (1), it can be deduced that for the same energy density, thicker target corresponds to smaller temperature change, which is not preferable for observation. So, the material and the thickness of the target should be selected carefully, sometimes it needs to make a compromise, in order to get good sensitivity. The longer range of electrons leads to lower power density deposition in the target, so the possibility of target ablation, which largely confines the application of this method to IPIB under the same cross-sectional energy density, is considerably low. However, lower power density may lead to obviously lateral heat transfer. Larger error will be introduced in this way. It is formidable for direct observation of IPEB stopping process in the target. So, modeling was used for verification. The 2-D axisymmetric heat transfer in a target was simulated to estimate the process of thermal equilibrium between the two surfaces of the target. The power density distribution formed by IPEB irradiation was approximated as

$$P(x, y, z, t) = d(z) \cdot U(x, y) \cdot g(t), \tag{2}$$

in which $P(x, y, z, t)$ is the beam power density distribution on the target, $d(z)$ is the depth-normalized energy loss distribution vs. the depth z, $U(x, y)$ is the cross-sectional beam energy density distribution function on the x-y plane, and $g(t)$ is the time-normalized power evolution function that can be estimated from the beam current curve acquired by the Faraday cup.

$d(z)$ can be deduced from the electron stopping power dE/dz. In this work, it was calculated with Monte Carlo particle transportation code FLUKA.[11] $U(x, y)$ can be measured by diagnostic method such as calorimeters and infrared diagnostics. For verification purpose, here we took the form $\exp(-r^2/3)$ for $U(x, y)$. As the emission of IPEB current density in the diode follows the Child-Langmuir Law (i.e., the three-halves-power Law),

$$J_e = \frac{4\varepsilon_0\sqrt{2e}}{9\sqrt{m_e}} \cdot \frac{U^{3/2}}{(d_0 - v \cdot t)^2}, \tag{3}$$

in which U is the accelerating voltage, d_0 is the initial anode-cathode gap, ε_0 is the vacuum permittivity, v is the plasma expansion velocity, m_e is the electron mass, and e is the electron charge. It is inferred that the working voltage waveform of the diode has a flattop near the highest voltage and this leads to much stronger emission than at the low voltage section, so assuming the IPEB as monoenergetic is acceptable.

In 2-D axisymmetric system, the temperature T at time t and position (r, z) is calculated by solving the Fourier thermal conduction equation. The differential equation is

$$\rho C_V \frac{\partial T}{\partial t} = \lambda \left(\frac{\partial^2 T}{\partial r^2} + \frac{1}{r}\frac{\partial T}{\partial r} + \frac{\partial^2 T}{\partial z^2} \right) + P, \tag{4}$$

where ρ, C_V, and λ are the density, specific heat, and thermal conductivity of the target, respectively. For initial condition, we take

$$T(r, z, 0) = T_0, \tag{5}$$

where T_0 is 298 K.

For boundary condition, in order to evaluate the energy loss by infrared radiation, the Stefan-Boltzmann boundary condition was taken

$$j = \varepsilon\sigma(T^4 - T_0^4), \tag{6}$$

in which j is the surface-to-ambient radiative heat flux, σ is the Stefan-Boltzmann constant, and ε is the emissivity, for the rear side of the target, $\varepsilon = 0.9$ and for the front side, $\varepsilon = 0.3$. As the air pressure in the testing chamber is quite low ($\sim 10^{-2}$ Pa) and no ablation or vaporization occurs, convective thermal transfer was not taken into account.

In order to simulate the heat transfer in a time scale from tens of ns to several hundred μs, a multi-step tactic was used as in the first five hundred ns when exists IPEB power injection, the time step of the calculation was 0.1 ns to ensure the accuracy. In the exceeding 0.2 ms, a time step of 0.1 μs was taken with a view to save computing time and memory. The equation is solved by the finite element method (FEM) software Comsol Multiphysics.

III. EXPERIMENTAL

The infrared imaging experiment was carried out on pulsed electron accelerator BIPPAB-450. The accelerator uses a magneto generator to generate a high voltage pulse up to 250 keV, and then, the pulse is rectified by a water-filled Blumlein line to form an 80 ns pulse (FWHM) and then

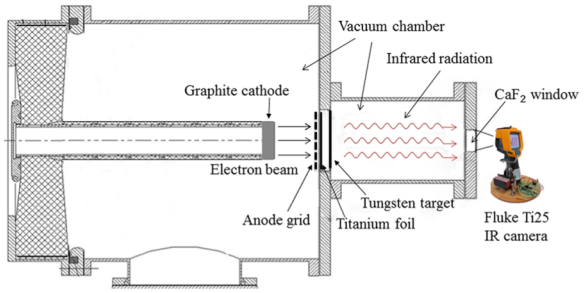

FIG. 1. Schematic diagram of the infrared imaging diagnostic system for IPEB.

voltage doubled by an autotransformer. IPEB is generated with a diode with explosive emission:[12] pulsed negative voltage is applied to a 45 mm-diameter graphite cathode, dense plasma is formed, and then the electrons are accelerated to form IPEB. A supporting metal grid with transparency of over 95% and a 50-μm-thick titanium foil was used as anode and a 100-μm-thick tungsten film painted with lusterless acrylic coating on the rear surface was placed 10 mm downstream as the infrared target. The whole set was positioned in a chamber evacuated from apertures on the anode to minimize the effect of convective cooling. The infrared image was captured through a CaF_2 window by a Fluke Ti-25 thermal camera triggered by an electronic-controlled robot arm (see Fig. 1). The images were captured in less than 0.1 s after IPEB emission. Working parameters of the accelerator, such as diode voltage, current, and the IPEB beam current, were measured by a voltage divider, Rogowski coil, and Faraday cup[13] correspondingly (see Fig. 2). The electrical signals acquired from the above sensors were recorded with a Tektronix TDS 2024 oscilloscope.

IV. RESULTS AND DISCUSSION

A. Validation of experimental apparatus

As discussed in previous research, infrared targets with low electron stopping power, such as stainless steel and copper may fail to stop the electrons completely. In this case, the infrared window placed downstream may be damaged by the electron beam. To avoid this, tungsten is selected as the target

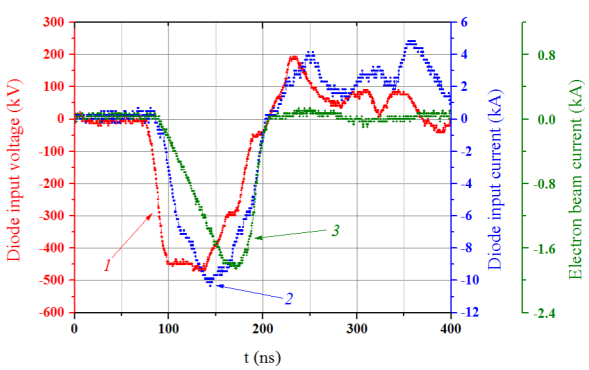

FIG. 2. Oscilloscope graphics of the voltage (1) and current (2) applied on the cathode and the total current of IPEB (3).

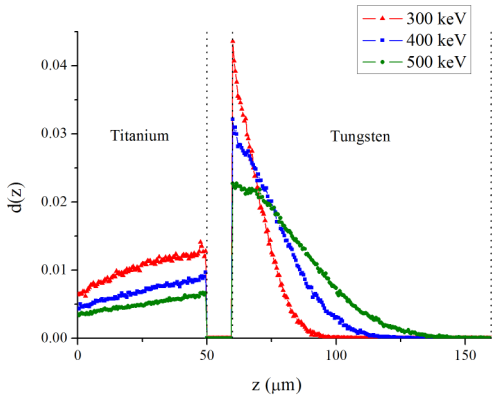

FIG. 3. Depth-normalized energy loss function of electrons in 50 μm titanium and 100 μm tungsten.

material. Fig. 3 shows the normalized electron energy loss function in 50-μm-thick titanium and 100-μm-thick tungsten. 10 μm of vacuum is set between two films to simulate the space between them. As demonstrated in Fig. 3, 500 keV electrons can be completely stopped in the tungsten film. It is also manifested that with higher electron energy, lower portion of the electron beam energy deposits in the titanium window. That means, higher electron energy is more favorable to the cooling of the anode, meanwhile it achieves higher energy efficiency in the window system and is thus more preferred in applications.

As the bremsstrahlung radiation of electrons is much stronger than ions, special attention must be given to the radiation protection of sensor apparatus. Fig. 4 shows the photon fluence of a 3-cm-radius, 450 keV electron beam along $z+$ axis on 50 μm of titanium, and 100 μm of tungsten placed near the $z = 0$ plane (simulated by FLUKA). It can be estimated that additional protection must be added for the personnel and in this research, besides the protection of the steel structures (the hull of vacuum chamber, the autotransformer, and the Blumlein line) and a 40 cm concrete wall, 3 mm of lead was used to enhance the operating position of accelerator. Electronic equipment: the infrared camera, the robot arm, and its subsidiary circuit are exposed to the bremsstrahlung γ-ray and they worked normally.

Considering the efficiency of the window, a calibration curve was utilized to calculate the actual temperature on the

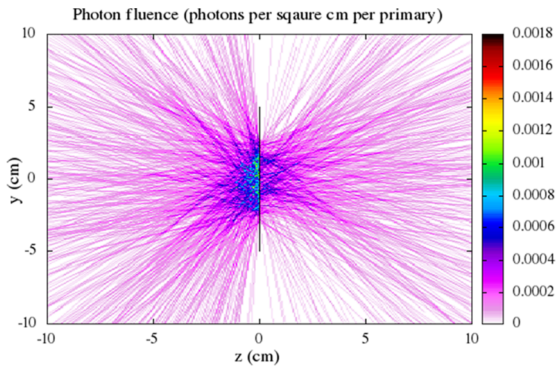

FIG. 4. Bremsstrahlung photon fluence of 450 keV electron injecting on 50 μm titanium and 100 μm tungsten.

rear side of the target. The fitted calibration formula of the CaF_2 window is

$$T_1 = 0.3328 \cdot T_2 + 7.8627, \quad (7)$$

where T_1 stands for the temperature measured by the infrared camera and T_2 is the actual temperature on the target surface. The temperature converting curve of the infrared window was also utilized to check the influence of irradiation. For CaF_2 window, the infrared transmittance remained virtually unchanged after more than 200 shots. However, as claimed by our co-researchers in another laboratory, a ZnSe infrared window underwent noticeable decrease in transmittance after tens of shots in IPIB tests. Although the exact mechanism is difficult to determine, it is quite possible that the radiation resistance of ZnSe is inadequate.

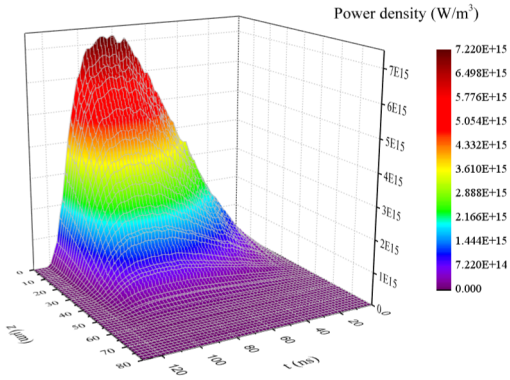

FIG. 5. Power density distribution in tungsten target with IPEB energy density 1 J/cm^2.

B. Temperature field simulation

In the source term of the temperature field simulation, the normalization of IPEB beam current (curve 3 in Fig. 2) was taken as $g(t)$; the normalized electron energy loss of 400 keV (normalization of the right part of the electron energy loss function in Fig. 3) vs. the depth was adopted as $d(z)$. In the center of the target, the energy density of IPEB is 1 J/cm^2 and decays following $\exp(-r^2/3)$ along the $r+$ direction.

Fig. 5 shows the incident power density of IPEB in the center ($r = 0$) of the target. As the energy of the beam is compressed by short pulse and electron range, the peak value of the power density can reach the order of 10^{15} W/m^3. With direct energy deposition, the injected energy flux is much larger than conductive heat flux, so the temperature in the target increases sharply in the first 100 ns.

During the first 500 ns of the temperature field evolution (Fig. 6), despite that the maximum temperature rise is only 160 K, which is much lower than that caused by IPIB with the same particle energy and beam flux, the temperature changing rate can still reach the order of 10^9 K/s, considering the short period. For this small temperature increase, the energy loss caused by heat irradiation from the surface is negligible. It is also demonstrated that along the depth, the temperature field expansion is confined within 40 μm and this means that the energy injection, rather than heat conduction is the dominating effect. During this period, the lateral expansion of the temperature field is comparatively weak because the

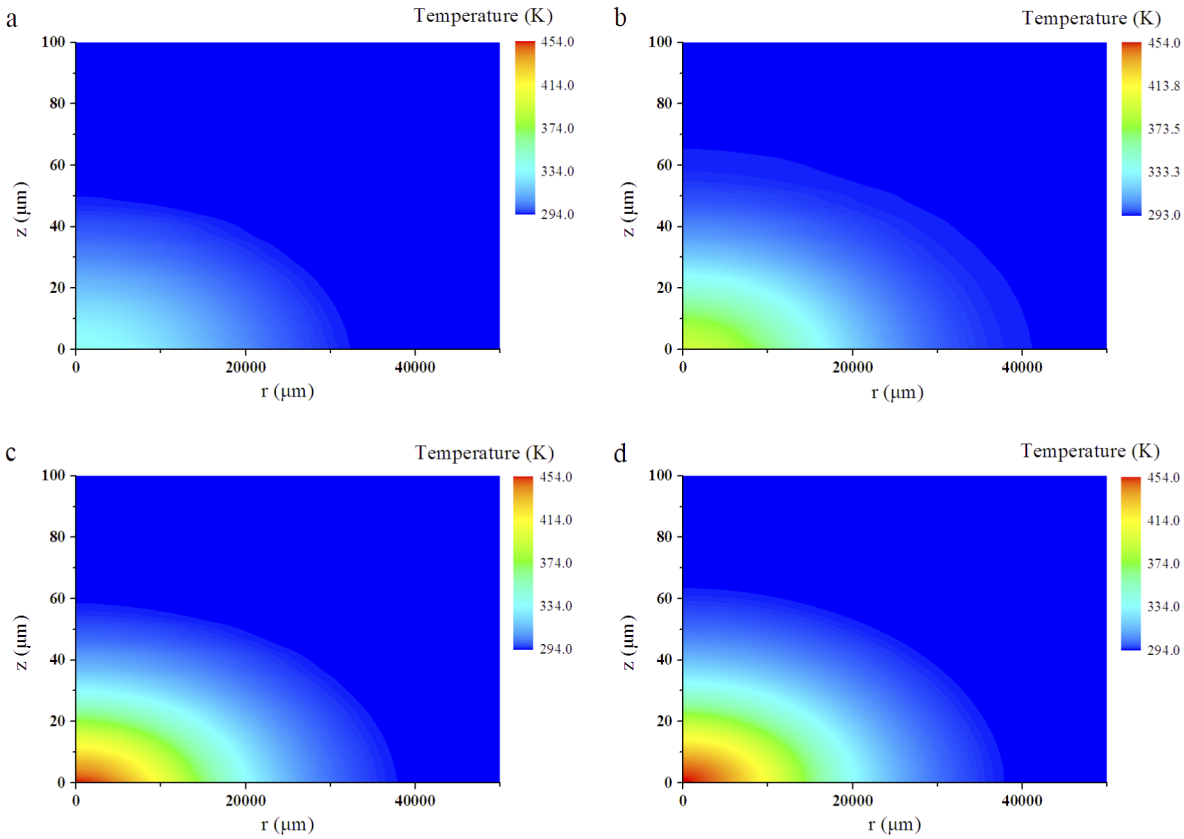

FIG. 6. Temperature distribution evolution in the first 500 ns: (a) 50 ns, (b) 75 ns, (c) 100 ns, and (d) 500 ns.

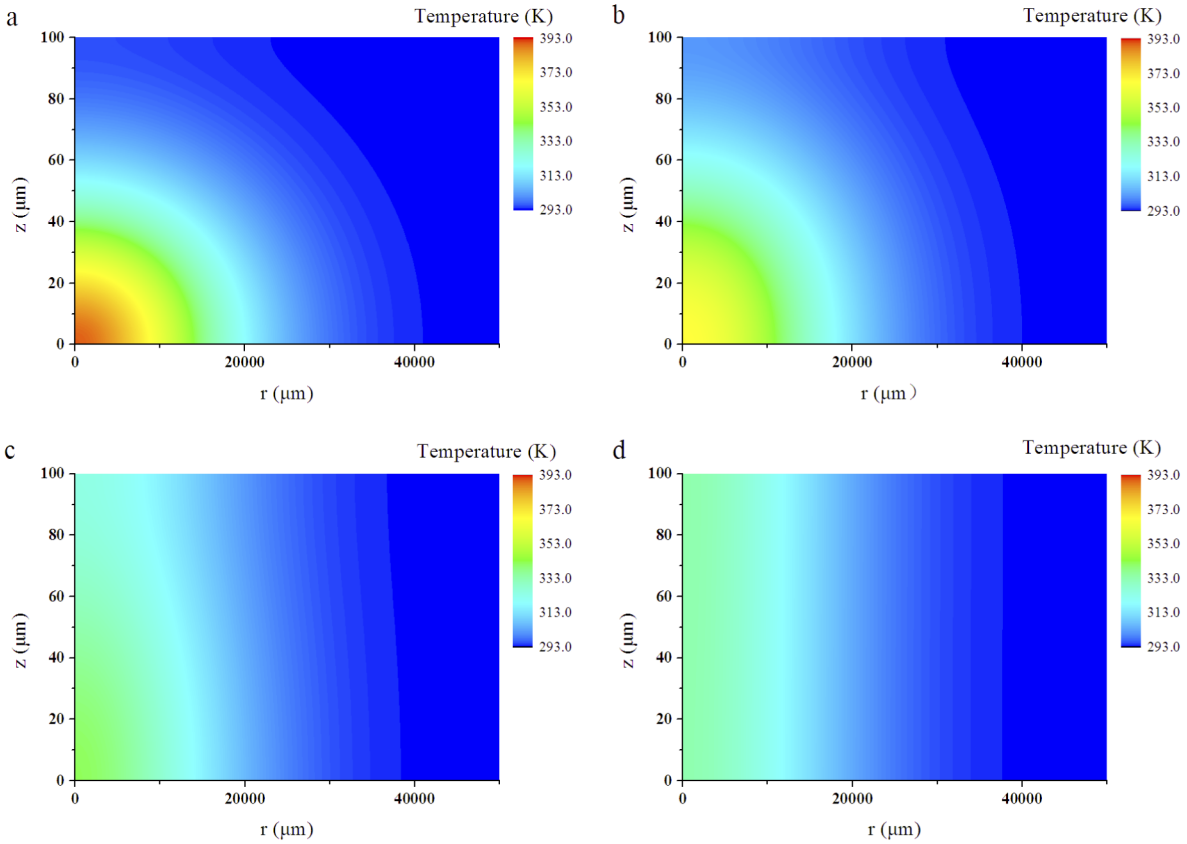

FIG. 7. Temperature distribution evolution in the succeeding 0.2 ms: (a) 5 μs, (b) 10 μs, (c) 30 μs, and (d) 0.1 ms.

power density gradient along the depth is much greater than the one along the radius.

Fig. 7 shows the temperature field distribution in the succeeding 0.1 ms. In less than 30 μs, the temperature field has expanded to the rear surface of the target. At 0.2 ms, the temperature difference of the points with the same radius at the front and the rear surfaces is less than 0.05 K. This means that the thermal equilibrium has been established, when taking temperature resolution of the camera into account, between the two surfaces. And for infrared imaging diagnostics, 0.2 ms is a proper time delay between IPEB shooting and infrared image capturing. With longer time delay, the error caused by lateral thermal conduction will be larger and the thermal transfer process afterwards can be described with thin shell heat transfer modeling as previously studied.[9]

With the data at 0.2 ms, the calculated IPEB energy density at the center of the target is 0.9812 J/cm^2, which means as a result of lateral thermal conduction, an error of 1.88% is caused. After this period, the heat transfer in the target can be described on the x-y plane, regardless of heat conducting in z direction. Such simulation of the temperature was carried out in the following 0.1 s and showed that in the center, a temperature decrease of 1.2 K was caused. It means that an extra error of 3% was caused by the delay in image capture.

Also, by analyzing the temperature evolution in the center (r = 0) on the front and rear surfaces (see Fig. 8), we can see that during the irradiation, rising of the temperature can reach the rate of 10^9 K/s, which is largely caused by high power density injection. However, after irradiation, the temperature change rate, driven by the temperature gradient, is much lower (10^7 K/s or less) as a result of relatively small temperature gradient caused by IPEB.

C. Thermal imaging experiments

IPEB infrared imaging experiments were conducted with changed diode anode-cathode gaps ranging from 8 mm to 20 mm. Captured infrared images were analyzed with software SmartView (see Figs. 9(a)–9(d)). Geometrical conversion was imposed with the angle of view and the apparatus size. Before the shooting of IPEB, an image of the cold target (as in Fig. 9(a)) was captured as the base temperature field. Then,

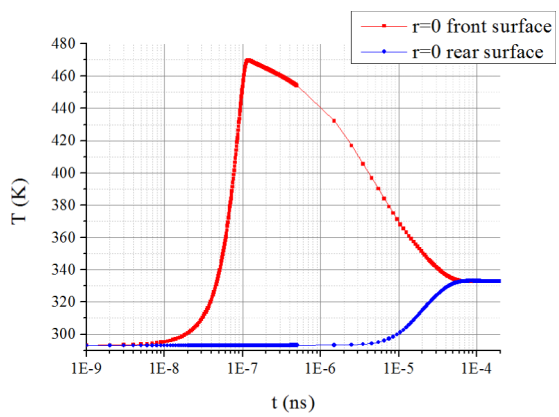

FIG. 8. Temperature evolution of the central points on the front and rear surfaces.

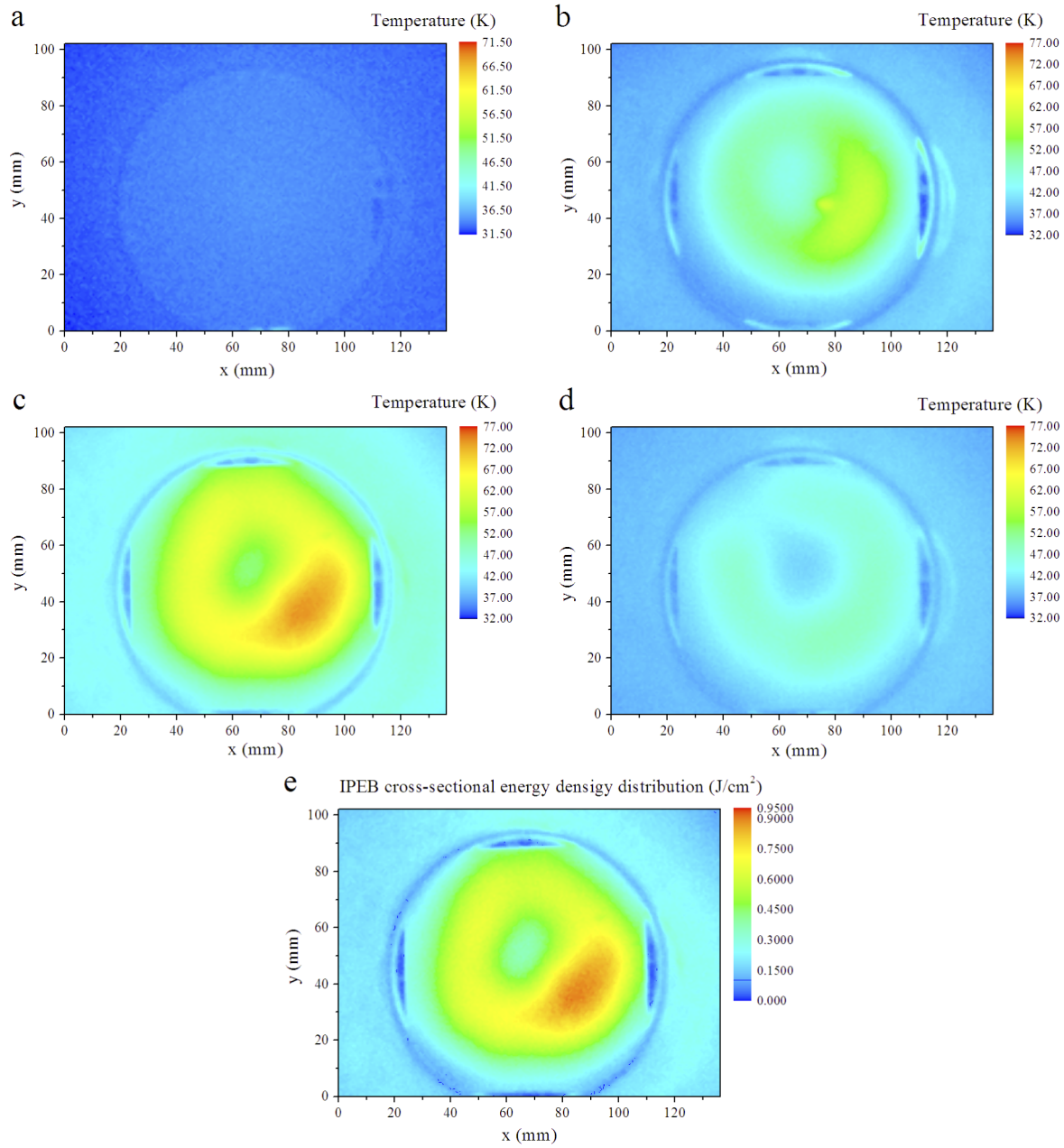

FIG. 9. Results of infrared imaging experiments: (a) infrared image before irradiation, and infrared images with different anode-cathode gaps: (b) 12 mm, (c) 16 mm, (d) 18 mm, and (e) cross-sectional energy distribution calculated from Fig. 9(c).

by calculating the temperature difference caused by IPEB pulse, the cross-sectional energy distribution was calculated with Eq. (1). As the temperature resolution of the camera is 0.1 K, by taking a conversion with Eqs. (1) and (7), an energy resolution of better than 0.1 J was achieved. In the experimental sets, 1 mm on the tungsten target corresponds to slightly more than 1 pixel in the camera sensors; consequently, the spatial resolution is 1 mm for this system.

The cathode emission properties of the diode were analyzed with the infrared images. As can be observed in Figs. 9(a)–9(d), as the anode-cathode gap changes, the output energy of the diode varies notably as the impedance of the diode changes. The uniformity of the diode can be also characterized by the images. It is shown that for various anode-cathode gaps, the emission of IPEB is relatively stronger at the lower right region of the cathode. A possible explanation to this phenomenon is that the anode foil may have a deformation in this part and a narrower diode gap is formed in this way. A smaller diode gap means a much stronger electric field. The explosive emission, which greatly relies on the electric field intensity, is enhanced and makes more intense plasma generation.

The stability and energy efficiency of the diode were also analyzed with the infrared images. For each diode gap, a series of pulses were shot for the test. The energy of an IPEB pulse was calculated by integrating the cross-sectional energy density. The input energy of the diode was calculated by integrating the product of the diode voltage and the diode input current. In our experiments, the input energy of the diode is 105.78 J ± 4.92%. Whereas for IPEB, the common

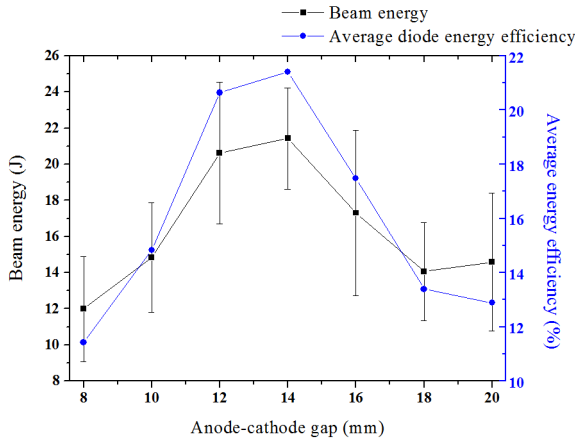

FIG. 10. The output energy of IPEB and the average energy efficiency of diode.

instability of total beam energy is about 25% (see Fig. 10); this implies that the diode is the main factor contributing to the fluctuations in the output parameter. It is revealed that the highest diode output and energy efficiency were achieved at a diode gap of 14 mm, which means that the impedances are well matched between the diode and the front-end circuit. With changed diode gap, both output and efficiency of the diode reduce rapidly.

D itge h rapidossibl 6 oup trimiztions 6 ouf 6 the ome trhod T 6 . 6 6 Tf 8 . . Td W

tho 6 abe 6 aused 6 tn 6 rlo tacuum 6 t aor ng 86 contdiions T g G g G g G g